Thermal-Mechanical Model of Depression Formation in Steel Continuous Casting

Matthew L.S. Zappulla and Brian G. Thomas

Abstract Many serious defects in the continuous casting of steel, including surface cracks and depressions, are related to thermal-mechanical behavior during solidification in the mold. A finite-element model has been developed to simulate the temperature, stress, and shape of the steel shell near the strand surface, as it moves down the mold at the casting speed in a state of generalized plane strain. The thermal model simulates transient heat transfer in the solidifying steel and between the shell and the mold wall. It is coupled with a stress model that features temperature-, composition-, and phase-dependent thermal-elastic-visco-plastic constitutive behavior of the steel. Depressions are predicted to form when the shell is subjected to either excessive compression or tension, but the shapes differ. Predicted depression shapes are compared with previous plant observations. The model reveals new insights into the mechanisms of surface depressions and longitudinal cracks in this process.

Keywords Steel · Solidification · Finite element · Depression · Crack · Modeling

M.L.S. Zappulla · B.G. Thomas (✉)
Formerly with Department of Mechanical Science and Engineering, University of Illinois at Urbana-Champaign, Champaign, USA
e-mail: bgthomas@illinois.edu

M.L.S. Zappulla
e-mail: zappull1@illinois.edu

M.L.S. Zappulla · B.G. Thomas
Department of Mechanical Engineering, Colorado School of Mines, 1610 Illinois St., Golden, CO 80401, USA

The Minerals, Metals & Materials Society, *TMS 2017 146th Annual Meeting & Exhibition Supplemental Proceedings*, The Minerals, Metals & Materials Series,
DOI 10.1007/978-3-319-51493-2_48

Introduction

In continuous casting, initial solidification behavior within the mold is of the utmost importance. Defects or inconsistencies that appear within the first meter or less of the casting directly affect surface quality in substantial ways. In an ideal situation, adequate machine and narrow face tapering of a caster ensures uniform heat transfer between the mold and steel strand. However, in practice this can be difficult to implement for a variety of reasons. Insufficient taper may lead to reduced or non-uniform heat transfer between the strand and the mold; this can result in narrow face bulging, corner rotation, and shell thinning [1]. Excessive taper causes accelerated mold wear, and possibly even buckling of the shell [1]. Both of these taper issues can cause gutter, longitudinal cracks, and even breakouts [1].

Cracks are one of the most costly defects in continuous casting, often resulting in scarfing, downgrading, or in the worst case scenario, rejection or failure of final products. They arise due to excessive tensile stress together with metallurgical embrittlement. Although the general causes are known, determining the detailed fundamental steps of formation of particular defects and the corresponding best solution(s) remains very difficult. By investigating the effect of different temperature and mechanical histories using computational models, this work aims to identify specific caster situations and conditions that can lead to the formation of different types of surface cracks and the distinguishing depressions that accompany them.

There has been significant previous work to develop damage criteria for hot-tear crack formation [2–5], hot ductility [6–9], strain to failure [10], and sensitivity to cracks [11, 12]. Recent work has examined solidification cracks [12], focusing on micro-scale phenomena. Previous thermal-mechanical modeling suggested that cracks during thin-slab casting with a funnel mold were due to bending around the funnel curves while the shell was still weak [13].

Much recent literature is concerned with the micro-scale phenomena and compositional effects related to cracking [12, 14–16]. Previous work with a macro-scale thermal-mechanical model suggested how off-corner gutter depressions form [1]; however, work on longitudinal and transverse cracks and their associated depressions is rare. More work is needed to understand the fundamental mechanism(s) of depression formation and the steps that can be taken when troubleshooting a caster to solve a particular surface-defect problem. Quantitative answers are needed to questions such as: When does a crack form without a depression? When does a depression form without a crack? When does a sub-surface crack form and propagate (or not) to the surface? What plant practices lead to a given type of crack and shape of depression?

Cracks and depressions are clearly related to each other. Figure 1 shows a few examples of cracks and depressions from different steel plants and previous literature. The wide range of different shapes of the surface defects in these images suggests different formation mechanisms. For example, when a crack opens at the base of a depression it changes the characteristic shape of the defect. Even labeling a given defect is difficult, because words such as gouge, depression, void, crack,

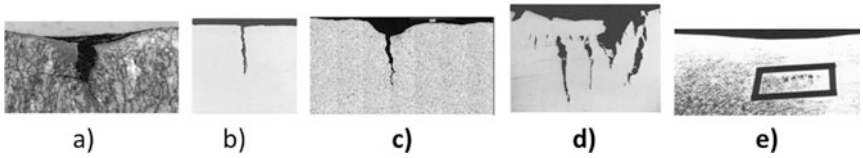

Fig. 1 Observed types of surface defect shapes and openings: **a** depression with high aspect ratio opening, **b** surface crack with no depression [17], **c** depression with narrow opening above crack, **d** depression with multiple sub-surface cracks [17], **e** depression with only subsurface cracks [1]

opened crack, etc. depend on the formation mechanism, which is generally not known and often involves several different stages.

Model Description

The steel solidification process was simulated in this work using a computational thermal-mechanical model [18, 19] of a 2-D slice in a state of generalized plane strain, to predict the displacement, strain, and stress histories of the shell. The governing equations are solved using the finite-element method in ABAQUS/Standard (implicit) [20]. The transient analysis was performed in two steps consisting of a heat transfer analysis, followed by a mechanical analysis. The simulation domain shown in Fig. 2 is a representative portion of the solidifying steel located somewhere along the broad face away from the corner region, where a local surface defect might form. For simplicity, the depression center can modeled as a symmetry plane, and the other edge with a generalized plane strain condition and subjected to fixed displacement.

Heat flux leaving the domain bottom in the region of good (uniform 100%) contact with the mold is given as follows [18, 19], and is applied using user subroutine DFLUX in ABAQUS [20].

$$\dot{q}_{standard} = 6.36(t + 1.032)^{-0.5} \tag{1}$$

The applied heat flux ramps down linearly from 100% at 5 mm to 50% at the depression center, from 1 s to 3 s, as shown in Fig. 3. This is followed by a further linear decrease to 20% at crack center, over a widening region that increases linearly from 5 mm at 3 s to 20 mm wide at 10 s.

The material properties for this study are for a typical low carbon steel grade (0.045 wt%C) used in previous work [18, 19]. Composition and phase transition temperatures are given in Tables 1 and 2.

Temperature- and carbon-dependent properties: enthalpy [21], thermal conductivity [22], density [23, 24], thermal linear expansion [21], and Young's modulus [25] for this steel grade are based on the phase fractions given in Fig. 4. Details of the property data can be found in Sect. 2.7 of [19]. The elastic visco-plastic

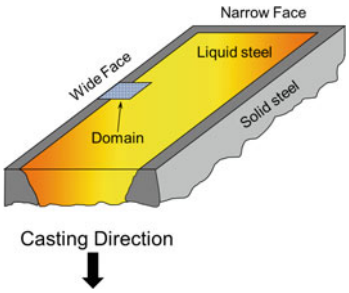

Fig. 2 Solidification of a continuous cast slab (cutaway) showing model domain

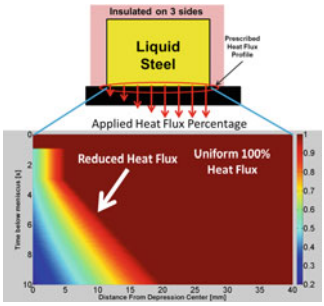

Fig. 3 Thermal boundary conditions and reduced heat transfer applied on domain

Table 1 Low carbon steel composition (wt%C)

Steel	C	Mn	Si	S	P	Cr	Ni	Al	Ti	Cu
Low carbon	0.045	0.20	0.015	0.01	0.01	0.01	0.01	0.04	0.05	0.01

Table 2 Low carbon steel phase transition temperatures (°C)

Steel	Pour	Liquidus	Solidus	Mushy Range	δ start	δ end	γ start
Low carbon	1532	1528	1505	23	1505	1385	1418

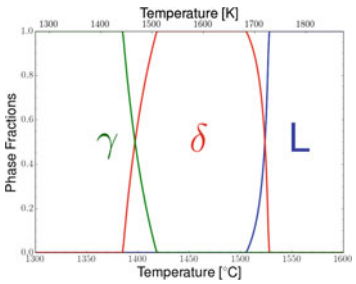

Fig. 4 Phase fractions for the low carbon steel grade examined [19]

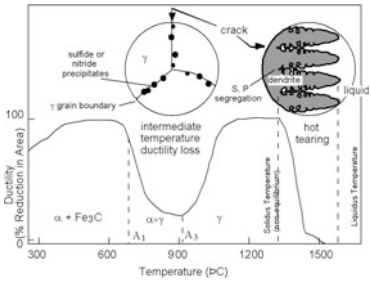

Fig. 5 Low ductility/high embrittlement regions of interest [8]

constitutive models used in this work include both strain-rate- dependent plasticity and time-dependent creep for each steel phase. The δ-ferrite is modeled with the Zhu Modified Power law [26], the austenite phase uses model III from Kozlowski [27], and the liquid phase is a low-strength elastic-plastic material, as described elsewhere [26, 28].

To evaluate the likelihood of crack formation, a damage criterion must be chosen. Most steels exhibit two low ductility troughs, one near the solidus temperature, and a second "intermediate-temperature" drop just above the A_3 temperature, as shown in Fig. 5. Near the solidus temperature, the interdendritic liquid has a strong effect on the ductility of the steel as it is only "mostly" solid. This region (solid fraction between 90–99%) is used to identify "weak areas" susceptible to hot tear cracks. Specifically we are interested when this region experiences high inelastic strain while in a state of tensile stress. Future work will explore more quantitative damage criteria.

Results and Discussion

As observed in the literature, a drop in surface heat flux causes a rise in shell temperature [29]. With uniform heat transfer, the entire surface experiences the same temperature history, given by the lowest line in Fig. 6. When heat flux drops beneath the depression, that part of the surface reheats by several hundred degrees, as observed in other lines in Fig. 6. It should be noted that the austenite layer growth is severely slowed, so that layer becomes much thinner beneath the depression.

Typical temperature contour results at 10 s are shown in the center frame of Fig. 7. The left and right frames show temperature contours in vertical slices through the shell at both the depression center and the region of uniform heat flux. Following these results vertically downwards visualizes the time histories of the temperature profile at these locations. The reduction of the austenite layer beneath the depression is readily apparent as the austenite layer at the depression center is 55% thinner than at the far field. The thickness of solid shell is reduced by only ~1.5 mm (17%).

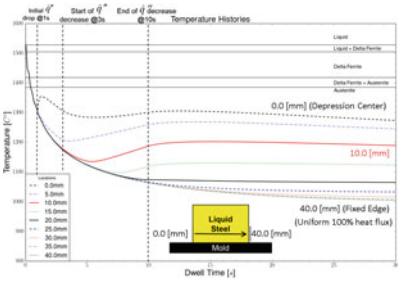

Fig. 6 Temperature histories across the domain surface

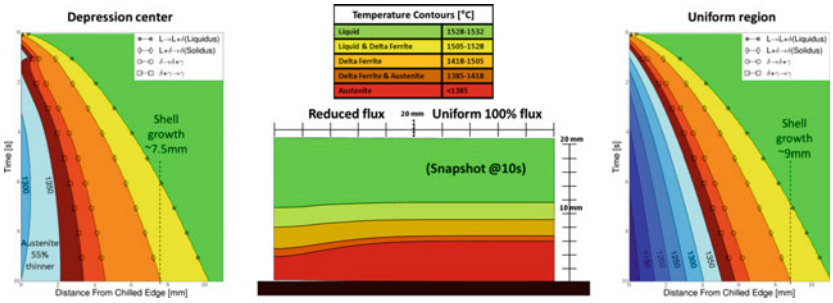

Fig. 7 Reduced heat transfer temperature contours, shell growth, and phase regions

Results for the ideal case of free shrinkage, except for friction at the shell/mold interface, are shown in Fig. 8a. With reduced heat transfer, the shell thins, and when stress concentrates locally, a slight U-shaped depression appears in the domain even without an externally applied force. The tension by friction at the mold interface in combination with the shrinkage of the rest of the shell causes the domain to neck and behave like a tension test specimen.

Results in Fig. 8b show the effect of a continuous applied tension (pull) on the domain edge for domains with different widths. These pull cases can occur in any situation where tension is induced on the shell by issues occurring somewhere outside the small domain; common reasons for this tension could be friction associated with mold flux infiltration problems or bulging due to inadequate taper. Increasing the applied tension results in a much deeper, but not necessarily wider, depression. Wider domains exhibit deeper depressions, for the same conditions.

Figure 9 shows a pull case where the shell was allowed to grow to 3 mm before the tension was applied to the domain. This is scaled along-side a depression from the work of Brimacombe [29] and shows a reasonable qualitative match. The necking formation mechanism is believed to be the predominant creator of depressions, due to the shape of the resulting U-shape depression which is commonly seen in practice.

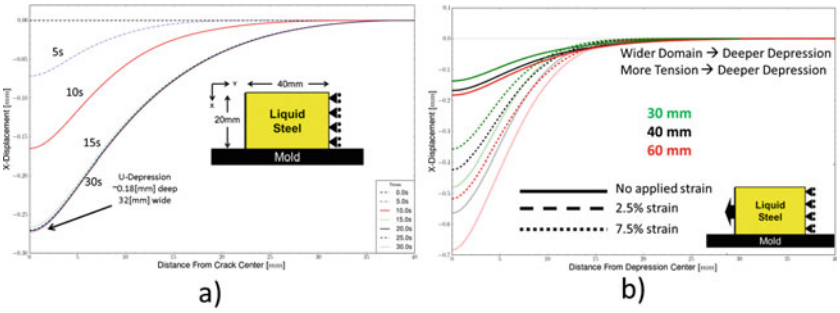

Fig. 8 **a** Formation history of a U-shaped depression (ideal shrinkage), **b** depression shape for different pull cases (10 s), showing effect of strain extent and domain size

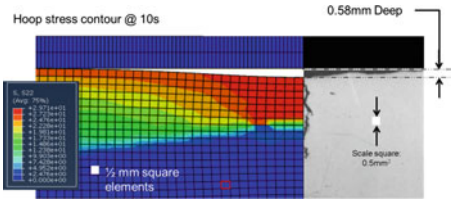

Fig. 9 Simulated necking depression shape (3 mm shell growth, 7.5% applied tensile strain) compared to literature (contours of stress perpendicular to solidification front)

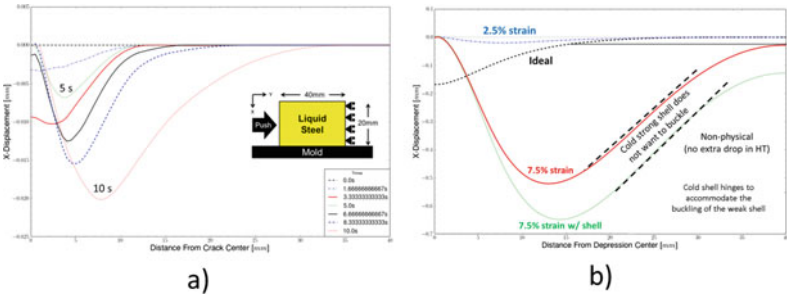

Fig. 10 **a** Formation history of a W-shaped depression, **b** depression shapes for different push cases

Figure 10 shows results for an applied compression (push) case. This situation could arise from an overtapered mold, where the narrow face mold may apply compression on the wide face shell in excess of the desired shrinkage of the strand. When the domain has compression applied to it, the surface of the shell buckles into a W-shaped depression. In the same way that increased tension results in a deeper U-shaped depression, increased compression causes a more severe W-shaped

depression. Low levels of compression (e.g., 2.5% case) produce very shallow depressions.

Figure 11 shows hoop stress contours for the severe push case with 7.5% applied strain. As the figure indicates, subsurface tension appears at the base of the W shape, right at the solidification front; this suggests the possibility of a hot tear at this location. W-shaped depressions are uncommon in plant practice; however, Fig. 12 shows a billet that appears to exhibit a W-depression.

Figure 12 is taken from the literature [30] and shows a billet removed from a caster. The caster experienced lubrication issues and became jammed in the mold: removal was accomplished by increasing the drive rolls until the billet finally came free. This resulted in what appears to be a W-shaped depression near the bottom of the photograph (see enlarged inset), caused by a buckling scenario due to the misfit between the solidifying shell and excessive taper of the mold. One possible reason that W-shaped depressions are uncommon in practice is suggested in the photograph. The generation of tension at the solidification front may cause a subsurface crack at the base of either of the two symmetrical depressions. Such a crack would relieve the stresses and might enable the W-depression to evolve into a single depression centered at the subsurface crack. As this crack could form at several places on either side of the W, the final shape of the single surface depression would be expected to wander, as observed in the top portion of Fig. 12. As the current model does not allow for cracks to form, this tension cannot be relieved in the same way that it may in the real process. Another possible reason for the rarity of

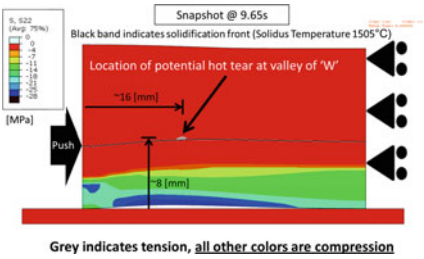

Fig. 11 Push case 7.5% strain hoop stress contours at 10 s

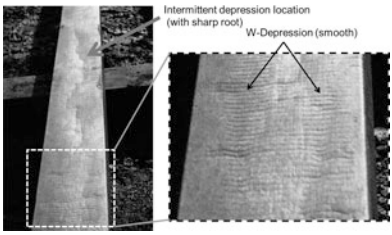

Fig. 12 Billet exhibiting signs of buckling depression mechanism [30, 31]

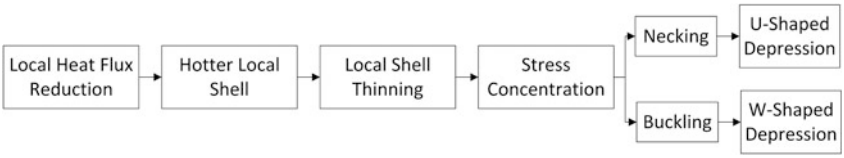

Fig. 13 Depression formation process

W-shaped depressions in practice is that the degree of compression required to buckle the shell in an appreciable way is quite high. Overtaper of only a few percent strain may cause a shallow W but it may be smoothed out in the drive/support rolls sub mold.

Conclusions

Results of this work suggest that there are two different mechanisms for depression formation in continuous casting, one with applied tension and one with applied compression. Additionally, these two mechanisms have quite different characteristic shapes and behaviors (see Fig. 13).

This work demonstrates that non-uniform heat transfer during initial solidification can lead to a depression even with ideal shrinkage (i.e., a perfectly tapered caster). This shows the importance of proper mold conditions regarding mold flux and mold surface upkeep. This work also suggests that the frictional interaction of the steel shell with the mold/flux in combination with shrinkage of the shell and imperfect mold taper can apply tension that could lead to depressions.

Future Work

Future work on this project is especially interested in collecting and characterizing cracks and depressions from operating casters. In addition, simulations will investigate these scenarios and the potential for air gap formation with a fully coupled model that includes detailed physics of the gap. Eventually, a full ¼ symmetry domain of a slab mold to include corner effects is desired as well as an implementation of a quantitative damage or crack criterion. Finally, surface defect modeling to explore grade effects especially into the peritectic range is desired.

Acknowledgements The authors wish to thank the members of the Continuous Casting Center at the Colorado School of Mines for their financial support, as well as the National Science Foundation, grant CMMI-13-00907 Blue Waters, and the National Center for Supercomputing Applications at The University of Illinois at Urbana-Champaign which is supported by the National Science Foundation (awards OCI-0725070 and ACI-1238993) and the state of Illinois.

References

1. B.G. Thomas, A. Moitra, and R. McDavid, Iron Steelmak. ISS Trans. **23**, 143 (1996)
2. M. Rappaz, J. Drezet, M. Gremaud, Metall. Mater. Trans. A **30A**, 449 (1999)
3. Y.M. Won, T. Yeo, D.J. Seol, K.H. Oh, Metall. Mater. Trans. B **31**, 779 (2000)
4. T.W. Clyne, G.J. Davies, Br. Foundrym. **74**, 65 (1981)
5. D.G. Eskin, L. Katgerman, Prog. Mater Sci. **49**, 629 (2004)
6. H.G. Suzuki, S. Nishimura, S. Yamaguchi, Trans. Iron Steel Inst. Jpn. **22**, 48 (1982)
7. P.J. Wray, Metall. Mater. Trans. A **15**, 2059 (1984)
8. B.G. Thomas, J.K. Brimacombe, I.V. Samarasekera, Trans. Iron Steel Soc. **7**, 7 (1986)
9. W.T. Lankford, Metall. Trans. **3**, 1331 (1972)
10. C.H. Yu, M. Suzuki, H. Shibata, T. Emi, ISIJ Int. **36**, S159 (1996)
11. B. Bottger, M. Apel, B. Santillana, D. Eskin, Metall. Mater. Trans. A **44**, 3765 (2013)
12. M.B. Santillana, Thermo-mechanical properties and cracking during solidification of thin slab cast steel. Ph.D. Thesis, Delft University of Technology, 2013
13. L.C. Hibbeler, B.G. Thomas, M.B. Santillana, A. Hamoen, A. Kamperman, in *European Continuous Casting Conference Associazione Italiana di Metallurgia, Riccione* (Italy, 2008)
14. S. Moon, The Peritectic phase transition and continuous casting practice, Ph.D. Thesis, University of Wollongong, 2015
15. M.M. Wolf, K. Kurz, Metall. Mater. Trans. B **12**, 85 (1981)
16. J. Konishi, M. Militzer, I.V. Samarasekera, J.K. Brimacombe, Metall. Mater. Trans. B **33B**, 413 (2002)
17. J.K. Brimacombe, F. Weinberg, E.B. Hawbolt, Metall. Trans. B **10**, 279 (1979)
18. M.L.S. Zappulla, L.C. Hibbeler, B.G. Thomas, Metall. Mater. Trans. A (2016 in review)
19. M.L.S. Zappulla, Grade effects on thermal-mechanical behavior during the initial solidification of continuously cast steels. M.S Thesis, The University of Illinois at Urbana-Champaign, 2016
20. ABAQUS 6.13 Theory Manual (DS SIMULIA Corp, Providence, RI, 2013)
21. K. Harste, Investigation of the shrinkage and the origin of mechanical tension during the solidification and successive cooling of cylindrical bars of fe-c alloys, Ph.D. Thesis, Technischen Universität Clausthal, 1989
22. K. Harste, K. Schwerdtfeger, ISIJ Int. **43**, 1011 (2003)
23. A. Jablonka, K. Harste, K. Schwerdtfeger, Steel Res. **62**, 24 (1991)
24. I. Jimbo, A.W. Cramb, Metall. Mater. Trans. B **24**, 5 (1993)
25. H. Mizukami, A. Yamanaka, T. Watanabe, ISIJ Int. **42**, 375 (2002)
26. C. Li, B.G. Thomas, Metall. Mater. Trans. B **35**, 1151 (2004)
27. P.F. Kozlowski, B.G. Thomas, J.A. Azzi, H. Wang, Metall. Mater. Trans. A **23A**, 903 (1992)
28. S. Koric, B.G. Thomas, J. Mater. Process. Technol. **197**, 408 (2008)
29. J.K. Brimacombe, F. Weinberg, E.B. Hawbolt, Metall. Mater. Trans. B **10**, 279 (1979)
30. C.A.M. Pinheiro, I.V. Samarasekera, J.K. Brimacombe, B. Howes, O. Gussias, Ironmak. Steelmak. **27**, 144 (2000)
31. I.V. Samarasekera, Private Communication (2015)